Solar Energy Materials and Solar Cells 201 (2019) 110119

Contents lists available at ScienceDirect

Solar Energy Materials and Solar Cells

journal homepage: www.elsevier.com/locate/solmat

In-situ composition analysis of photochromic yttrium oxy-hydride thin films under light illumination

M.V. Moro[a,*], D. Moldarev[a,b,c], C.C. You[c], E.M. Baba[c,d], S.Zh. Karazhanov[b,c], M. Wolff[a,b], D. Primetzhofer[a]

[a] Department of Physics and Astronomy, Uppsala University, Box 516, 751 20, Uppsala, Sweden
[b] Department of Material Science, Moscow Engineering Physics Institute, 115409s, Moscow, Russia
[c] Department of Solar Energy, Institute for Energy Technology, NO-2027, Kjeller, Norway
[d] Nano Science and Nano Engineering Department, Istanbul Technical University, 34469, Istanbul, Turkey

ARTICLE INFO

Keywords:
Yttrium oxy-hydride
Photochromic effect
In-situ ion beam analysis
Chemical composition

ABSTRACT

In this work, we investigate the chemical composition of a reactively sputtered photochromic YH_xO_y thin film by non-destructive ion beam-based techniques, i.e., Rutherford Backscattering Spectrometry, Particle-Induced X-Ray Emission, Time-of-Flight/Energy coincidence Elastic Recoil Detection Analysis and Elastic Backscattering Spectrometry. To enhance the accuracy of the analysis, the set of spectra was evaluated in an iterative self-consistent approach. This procedure resulted in high-resolution depth profiles of the chemical composition and revealed a thin oxygen-rich-layer on the surface, which apparently does not act as a self-passivation layer. In the film, the concentration of Y remains practically constant, whereas O replaces H during the oxidation process. In-situ light illumination was performed during the compositional analysis in a high vacuum setup. The results from these measurements demonstrate that, for these samples, the induced reversible photochromism is not linked to any detectable change in the bulk composition of the film and can thus take place even in a vacuum environment.

1. Introduction

The optical and electrical properties of yttrium hydrides (YH_x) strongly depend on the hydrogen concentration. Most prominent, this material undergoes a metal-to-insulator transition when x exceeds a specific value [1]. This transition triggers a rapid change of the physical properties, which can be used to study hydrogen diffusion in solids and in switchable mirrors [2]. Recently, yttrium oxy-hydride (YH_xO_y) thin films have started to attract the attention of the scientific community, as they were found capable of a switchable photochromic response triggered by light illumination under ambient conditions [3]. These reversible transitions make them promising materials attractive for many technological applications, such as smart windows and sensors [4–6].

The possibility of altering the optical transmittance, band gap and the magnitude of the photochromic response by changing deposition conditions has been established for YH_xO_y films [7–9]. In our recent work, for YH_xO_y [10], and later by Cornelius et al., for MH_xO_y (M; = Sc, Y and Gd) [11] it was demonstrated for which specific stoichiometry of yttrium oxy-hydrides a photochromic behavior can be observed. For instance, it has been shown that YH_xO_y films are photochromic only for certain oxygen to yttrium ratios (δ) of $0.45 < \delta < 1.5$ [10].

However, since the photochromic films investigated so far are typically prepared by reactive magnetron sputtering in mixed argon-hydrogen atmosphere followed by uncontrolled oxidation, it is challenging to predict the final oxygen and hydrogen concentration in YH_xO_y. Moreover, compositional analysis of YHO films using Time-Of-Flight Elastic recoil Detection Analysis (ToF-ERDA) have shown a considerable amount of impurities ($\approx$5 at.%), whereas the presence of small amounts of metallic incorporation can drastically change optical properties in this kind of material [12].

Also the specific mechanism of the photochromic response of rare-earth oxyhydrides is not yet clarified, although a series of investigations indicate a connection to structural [11,13,14] and electronic modifications [15] of the material during light illumination. All these processes, might be linked to changes in composition.

As composition depth profiles of systems containing light and heavy species for all constituents simultaneously and in an absolute way is demanding, ion beam analysis (IBA) employing projectiles in the MeV regime is an attractive tool. Employing different ion species, geometries and energies, elemental depth-profiles can be obtained with high

* Corresponding author.
E-mail address: marcos.moro@physics.uu.se (M.V. Moro).

https://doi.org/10.1016/j.solmat.2019.110119
Received 14 January 2019; Received in revised form 1 August 2019; Accepted 5 August 2019
Available online 13 August 2019
0927-0248/

accuracy and often free from the need for references [16].

The focus of the present work is twofold: at first, highly accurate depth profiles of the chemical composition of a reactive sputter-deposited photochromic YH_xO_y thin film are obtained using different ion beam-based techniques in an iterative and self-consistent procedure. Based on this analysis, we perform an in-situ investigation of potential changes in the film composition to obtain a better understanding of mechanisms which can explain the photochromism of rare-earth oxy-hydrides. Specifically, we investigated the concentrations and depth profiles of atomic species present in the material during light illumination, i.e. while the material is undergoing photochromic transitions.

2. Methodology

2.1. Sample preparation

Transparent yttrium oxy-hydride thin films were deposited onto glass substrates (microscope slides, 76 × 26 mm and 1 mm thick) using a Leybold Optics A550V7 on-axis pulsed in-line dc magnetron-sputtering machine in a mixed argon-hydrogen atmosphere. The films were grown at room temperature, and the base pressure in the chamber prior depositions was $\approx 10^{-6}$ mbar. The Ar:H_2 gas ratio during the reactive growth was 4:1, and the total chamber pressure during deposition was $\approx 3 \times 10^{-2}$ mbar. Subsequent to the film growth, samples were removed from the sputtering chamber and exposed to air for oxidation. A schematic of the film synthesis is shown in Fig. 1 (a). More detailed information on the sample preparation can be found in Ref. [17].

The thin-film deposition, as described in Fig. 1 (a), is easy, reproducible and efficient to produce photochromic YH_xO_y materials. The initial stage of the samples is transparent and yellowish. The samples become dark after a few minutes under light illumination at ambient conditions. This darkening effect is apparent from Fig. 1 (b) for which the sample, initially yellowish, has been illuminated for 30 min using a LED lamp (wavelength ≈ 400 nm and intensity ≈ 10 mW/cm^2). No significant changes in photodarkening are observed after ≈30 min of illumination.

The same light source has been employed for all investigations presented here. During the photo-darkening, a reduction in transmittance of 10–40% is found depending on the H and O concentration (i.e., x and y), light intensity and exposure time. In Fig. 1 (c), typical optical transmittance spectra are shown for the relaxed film and after 30 min of illumination, both measured using a Perkin Elmer Lambda 35 UV/VIS Spectrometer in a scanning mode with probing light between [190 − 1100] nm.

2.2. Ion beam analysis

The composition of the YH_xO_y was investigated by means of four different non-destructive IBA methods: Rutherford Backscattering Spectrometry (RBS), Particle-Induced X-Ray Emission (PIXE), Time-of-Flight/Energy coincidence Elastic Recoil Detection Analysis (ToF-E ERDA) and Elastic Backscattering Spectrometry (EBS).

RBS is the most commonly employed IBA technique. Light projectiles with MeV-energy are directed on the sample, and the backscattered particles from the target atoms due to the Coulomb repulsion are detected [18]. While providing straightforward information due to well-known cross sections and scattering kinematics, such analysis becomes more demanding either in terms of sensitivity (when light elements are present in heavy matrixes) or in terms of the resolution (when several heavy elements are coexisting in the layer to be analyzed). In this situation, it is more convenient to employ other more complex IBA methods [19]. As an example, one can use PIXE as it relies on the detection of the emitted characteristic x-rays from target atom [20], and permits to quantify trace-amount of elements (usually Z > 11) with sensitivities reaching the ppm level.

For light species, two IBA techniques can be an alternative: ToF-E ERDA and EBS. For the former, Time-of-Flight/Energy coincidence measurements of target particles elastically recoiled from heavy primary ions with several tens MeV enables mass-resolved composition depth profiling without masking the signals of light constituents, and with almost equal sensitivity for all constituents [21]. In EBS, by using elevated projectile energies, resonant non-Rutherford cross sections can be accessed, enabling isotope-specific detection of light species [22].

2.3. Experimental setup

The IBA measurements were carried out at the Tandem Laboratory at Uppsala University, using the two different scattering chambers: The

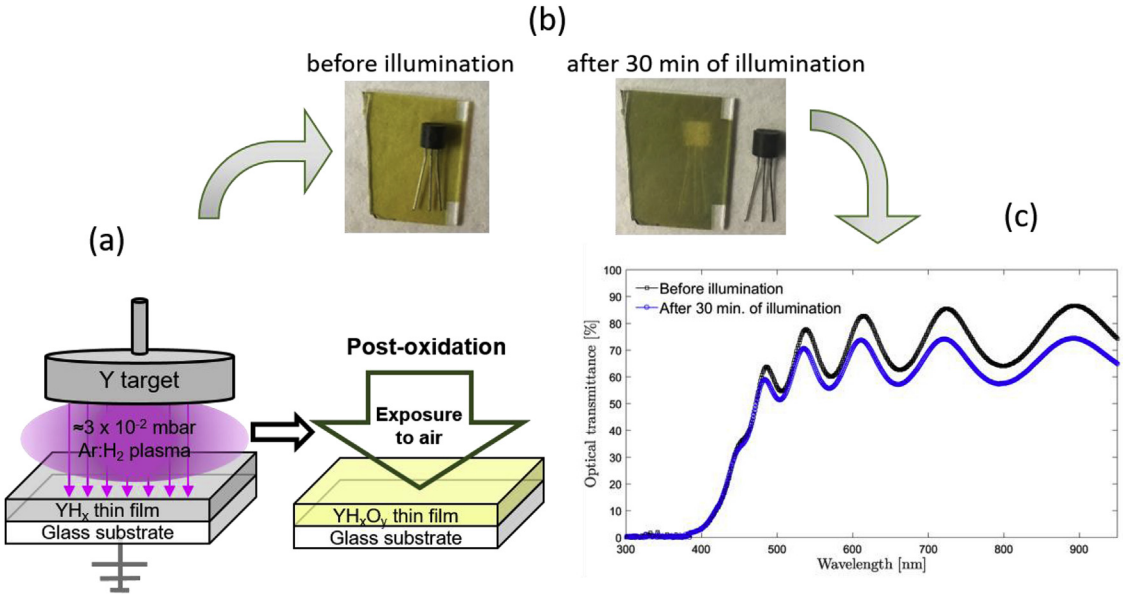

Fig. 1. (Color online). (a) Schematic drawing of the photochromic YHO film production by reactive magnetron sputtering. (b) Visual appearance of the photochromic sample studied in this work, before illumination (transparent/yellowish) and after a few min illumination (photo-darkened). (c) Corresponding reduction of optical transmittance (≈10%) constant for wavelengths larger than the absorption edge (≈450 nm): black line (before illumination) and blue line (after 30 min illumination).

first chamber features a passivated implanted planar silicon (PIPS) detector used for RBS and EBS analysis, as well as a silicon drift detector (SDD) used for PIXE. Both chambers are equipped with a telescope tube for ToF-E ERDA measurements, with the second chamber (employed in this study) containing an ionization gas detector chamber (GIC) for energy discrimination. Additionally, both chambers have sample-holders mounted on goniometers that are remotely controlled, which enables simultaneously data acquisition and sample positioning.

RBS and PIXE measurements were performed simultaneously using 2.0 MeV He^+ primary ions. The PIPS detector is placed at $\theta = 170^\circ$ scattering angle with resolution FWHM ≈13 keV for the whole detection chain. Previous x-ray diffraction analysis (XRD) on the sample indicated only small crystallites; hence, no residual channeling is expected. X-rays were detected by the SDD placed at $\theta = 135^\circ$ scattering angle. The X-ray SDD has a resolution of FWHM ≈136 eV for the Fe-K_α characteristic energy, and solid angle of $\Delta\Omega = (3.30 \pm 0.14)$ msr. A 79.5 μm Mylar absorber is placed in front of the detector Be-window (12.5 μm) to attenuate the low-energy characteristic x-rays (e.g., from Si) and Bremsstrahlung in order to decrease electronic dead-time and protect the detector from radiation damage due to backscattered particles.

For depth profiling all light constituents of the photochromic film, we used the ToF-E ERDA system of the second scattering chamber. As a probe beam, 36 MeV $^{127}I^{8+}$ ions were directed onto the sample under 67.5° with respect to the surface normal. The ToF-E telescope tube is fixed at 45° with respect to the ion beam. Further details of the setup can be found in Ref. [23]. The detection efficiency in the ToF-E detector - which differs from unity especially for light recoil species - has been corrected in the analysis code by semi-empirical values previously determined for our system [24]. For the ToF-E ERDA configuration used in this paper, the system presents a typical depth resolution of ≈50 nm, and a probing depth of ≈500 nm. It is known that irradiation with heavy primary ions can trigger the release of light species [25,26]. We counteracted any possible impact of sample degradation on the results by two strategies. At first, all data was recorded time-resolved, which permits to study compositional changes during the individual measurements. Additionally, to ensure consistency in the comparisons between the ToF-ERDA spectra and to reduce ion-beam induced hydrogen loss and pile-up effects, we kept similar charge-integration per irradiation spot, maintaining the beam current low and irradiating fresh sample surface for all consecutive ToF-ERDA measurement, when relevant.

In order to enhance quantification and depth-resolution on the thin oxygen-rich layer close to the surface, as initially identified by ToF-E ERDA (discussed in details in Sec. 3.1), EBS measurements were carried out using the elastic $^{16}O(\alpha,\alpha_0)^{16}O$ resonance at 3.037 MeV He^+ energy [27]. Since EBS resonant spectra are very sensitive to the specific beam energy, the projectile energy was increased in steps (starting from the energy corresponding to the resonance maximum) in order to depth-profile the oxygen concentration into the film. For an accurate oxygen depth-profile using EBS, the accelerator beam energy was before hands determined with an appropriate procedure [28], and the beam energy accuracy of each impinging projectile is known to be ≪ 0.5% for the whole He^+ energy used in this work.

3. Results and discussion

3.1. Iterative IBA

In Fig. 2, we present the results obtained from the different IBA-methods. In panel (a), the experimental RBS spectrum (black solid line) is shown together with a fit obtained by SIMNRA [29] (red solid line). In panel (b), the experimental PIXE spectrum (black solid line) is plotted together with a fit provided by GUPIX package [30] (red solid line). In panel (c), the ToF-E ERDA composition depth-profile deduced from a mass-energy spectrum (not shown) using the POTKU code [31] is presented. Finally, in panel (d), the depth-profile obtained from fits to several EBS spectra (not shown) using Multi-SIMNRA [32] is presented.

In Fig. 2 (a), the broad plateau at high energies ≈ [1100–1650] keV corresponds to the most prominent signal from the photochromic film in the RBS: yttrium. A priori, it would be possible to obtain a visually appealing fit to this spectral feature regardless the information from the other major constituents present in the film but less clearly observable or undetectable in RBS (i.e., O and H). However, such a fit would lead to an incorrect prediction of the thin-film thickness, as it would provide only an approximation to the areal density (in atoms/cm^2) of Y ignoring the other constituents. We thus employ different IBA methods and perform an iterative self-consistent approach during the evaluation: the key-information extractable from one technique is used as a boundary condition to another one, and the final fit for all spectra (achieved by chi-square minimization algorithms) leads to a description of the sample of interest with higher reliability.

The RBS fit shown in Fig. 2 (a) is based on the boundary condition of known relative concentrations of H and O obtained from ToF-E ERDA and EBS (discussed below), and the total areal density of the YHO film was found to be 5780×10^{15} at/cm^2 (≈790 nm assuming a weighted bulk density ≈ 4.49 g/cm^3). Additionally from RBS analysis, a trace-contamination of W (≈0.1 at.%) was found in the sample (see small feature at the highest energies up to ≈ 1850 keV in the RBS spectrum). Nevertheless, due to the poor mass-resolution of RBS for heavy elements, the unambiguous identification of the origin of this feature as W was done by PIXE (see the well-separated W-peak in Fig. 2 (b)). Furthermore, from PIXE analysis, trace-amounts of Ar (≈0.2 at.%) and Fe (≈0.05 at.%) were found in the sample. The other peaks in the PIXE spectrum (Si, K and Ca) are originating from the glass substrate.

In Fig. 2 (c), the ToF-E ERDA depth profile is presented. From this plot, one can see that close to the surface, i.e., in the region between ≈ [0–200] x 10^{15} at/cm^2, the oxygen concentration exceeds the one of hydrogen, in contrast to the film bulk ($> 200 \times 10^{15}$ at/cm^2). However, due to the limited energy resolution of the GIC detector and contributions from geometrical and energy loss straggling, an accurate analysis of the stoichiometry of this oxide layer is rather difficult. On the other hand, from this profile it becomes apparent that in the YHO bulk, the concentration of Y remains practically constant at ≈ 40 at.%, whereas the O signal slightly decreases (down to ≈ 20 at.%) and H concentrations increase (up to ≈ 40 at.%), which suggests that O replaces H during the oxidation process. This result is in agreement with other recent findings [10]. Also, some light-impurities (C and F at ≈ 1.5 at.%) were found. For the present ToF-E ERDA analysis, the depth-range shown in Fig. 2 (c) is limited to ≈ 3500×10^{15} at/cm^2, mainly due to limited range of recoiling species and multiple and plural scattering effects, which makes quantitative analysis at larger probing depth challenging.

In order to gain further insight in the nature of the thin oxide-layer on the surface of the YHO film and throughout the film bulk, in Fig. 2 (d), EBS depth-profile are presented. The EBS spectra were taken by increasing the helium primary energy in small steps (25 keV) from 3037 keV (oxygen resonance on surface) up to 3262 keV (oxygen resonance in the substrate-bulk). The recorded spectra for the different energies were analyzed iteratively using the Multi-SIMNRA code and considering prior knowledge from RBS, PIXE and ToF-E ERDA (latter for H concentrations - at least up to ≈ 3500×10^{15} at/cm^2), ensuring self-consistency. As one can see in Fig. 2 (d), the thin oxygen-rich layer (≈55 at.%) on the surface the YHO film presents an areal density of ≈203×10^{15} at./cm^2 (≈30 nm assuming Y_2O_3 density = 5.01 g/cm^3). The oxygen to yttrium ratio obtained for this sample was found to be $\delta \approx 0.7$, in perfect agreement with the compositional range of photochromic YHO samples reported in Ref. [10]. Furthermore, Fig. 2 (d) reveals a small gradient of O in the film (in accordance with ToF-E ERDA, panel (c)), showing that it extends until the interface film/substrate, which indicates an oxidation process which progresses throughout the entire YHO film upon exposure of the sample to air.

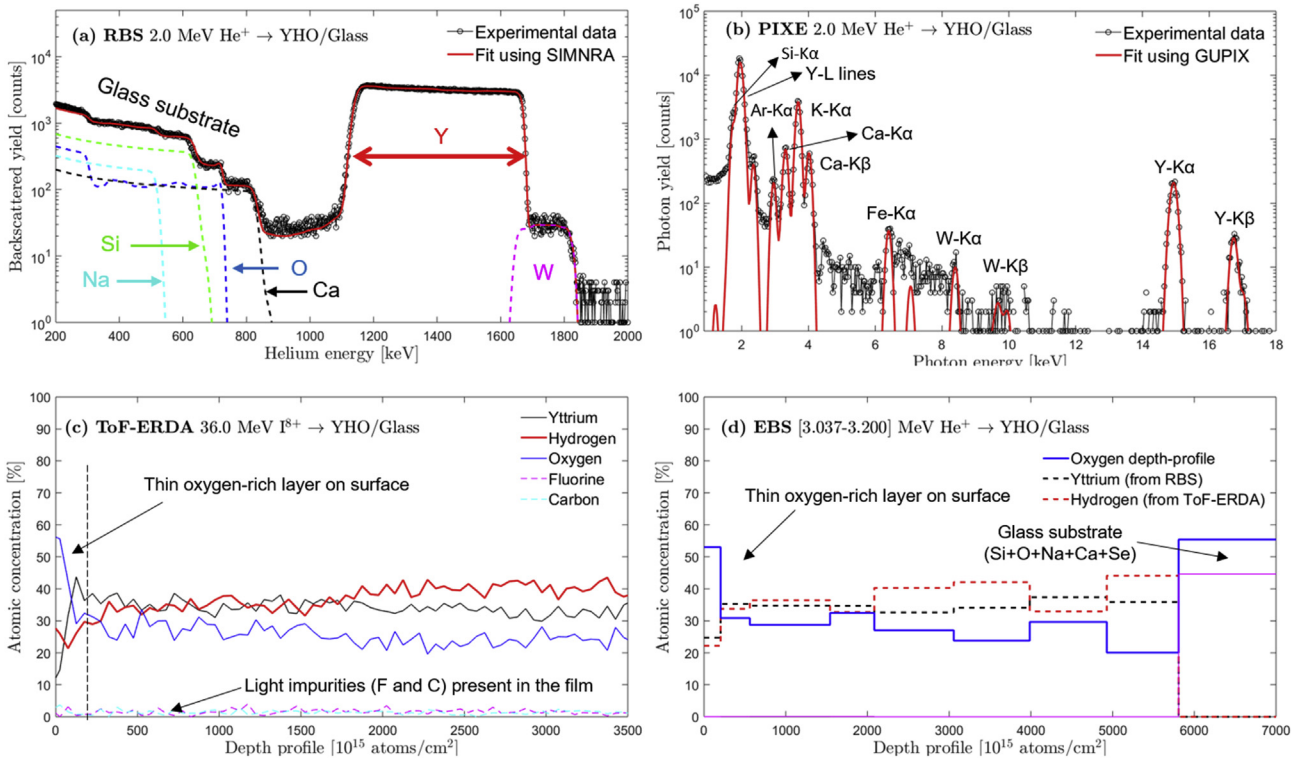

Fig. 2. (Color online). Summary of the IBA results. (a) Experimental RBS spectrum (black solid line) and the fit from SIMNRA (red line – other colors for constituents). (b) Experimental PIXE spectrum (black solid line) and the corresponding fit using GUPIX (red solid line). (c) Depth-profile obtained from a ToF-E ERDA analysis using POTKU. (d) Depth-profile deduced by fitting simultaneously several EBS spectra. (For interpretation of the references to color in this figure legend, the reader is referred to the Web version of this article.)

3.2. In-situ composition study

At present, no satisfying model describing the photochromism phenomenon in YHO exists. To obtain further knowledge on the mechanism, we have investigated possible chemical compositional changes of the YHO sample in-situ while triggering photochromism by external illumination. The sample was loaded onto the goniometer of the second scattering chamber (base pressure $\approx 1 \times 10^{-7}$ mbar). With the chamber initially kept dark, two ToF-E ERDA spectra were recorded (procedure similar to the one shown in Fig. 2 (c)). In sequence, the sample was illuminated through one of the chamber view-ports for 48 h in total. During the illumination, four ToF-E ERDA spectra were recorded: immediately after switching the light on, after 2 h, 44 h and 48 h of illumination, respectively. Subsequently, the lamp was switched-off, and the view-port was covered. After 2 h of relaxation time, two more spectra were recorded. Time-scales were chosen rather generous with respect to the typical darkening and relaxation times to account for possible effects of the high-vacuum environment.

In the following, the depth-profiles deduced from the ToF-E ERDA spectra are divided in two regions: the surface region ≈ [0–350] x 10^{15} at/cm^2, and the film bulk, ≈ [350–2000] x 10^{15} at/cm^2. Results for the depth-integrated Y, H and O values are shown in Fig. 3 (a) for the region close to the surface, and in (b) for the film bulk. There is no observable significant difference in the atomic concentration of Y, H and O before, during or after light illumination. The statistical uncertainty for concentrations of the main constituents Y, O and H from a single ERD-measurement performed in course of the present work, stemming mainly from counting statistics of the individual measurements and possible sample inhomogeneity, is estimated to be better than 2 at.% for the deduced Y, H and O values. Other systematic uncertainties (from, e.g., inaccuracies of the film stopping power and imperfections on the efficiency correction of the ToF-E system) are commonly estimated about 10–20% for a stand-alone ToF-E ERDA analysis. However, when evaluating relative concentrations in rather similar samples, their impact on results is negligible (see discussions in Ref. [33]). Note, that also the concentration gradients as shown in Fig. 2 (c) remained unchanged within the achievable accuracy and precision of the measurements. The specific results for the H, O and Y concentrations in the film, together with their respective cumulative statistical uncertainties before, during and after illumination are summarized in Table 1. From this data the maximum possible change in concentration of the potentially volatile species of hydrogen or oxygen in the bulk of the film due to illumination is found to be ≤ 1.1 at.%.

We want to point out that we exclude false negative result, i.e. no observable compositional changes due to a possible absence of photochromic transitions in high-vacuum. On the contrary, photo-darkening of the sample could be clearly observed in the high-vacuum environment. Moreover, when comparing the color of the YHO film upon photo-darkening in air and in high-vacuum, no visible difference in color is observed. This observation is in good agreement with both the ToF-ERDA results, indicating no compositional changes beyond ≈ 1 at. %, as well as qualitative considerations on the interaction with the residual gas in the experiment. From the base pressure of the vacuum chamber, no uptake of residual gas component at a rate larger than $\approx 0.1 \times 10^{15}$ atoms/sec is possible (assuming residual gas being exclusively hydrogen or oxygen, and a sticking coefficient of 1). Considering the areal concentrations of H and O in the film exceeding 1700×10^{15} at/cm^2, a significant uptake or release of species on a level of 60×10^{15} at/cm^2 is required to permit a change of 1% of the total areal density of the film. Any gas uptake/release at higher levels accompanied by the observed rather homogeneous distribution, i.e. requiring effective diffusion throughout the film, is considered highly unlikely. Additionally, also the pressure sensors of the equipment showed no pressure excursion, neither on switching on or off the light source. Altogether, the observed absence of significant uptake or release of either O or H by the bulk of the film (at a level > 1 at.%)

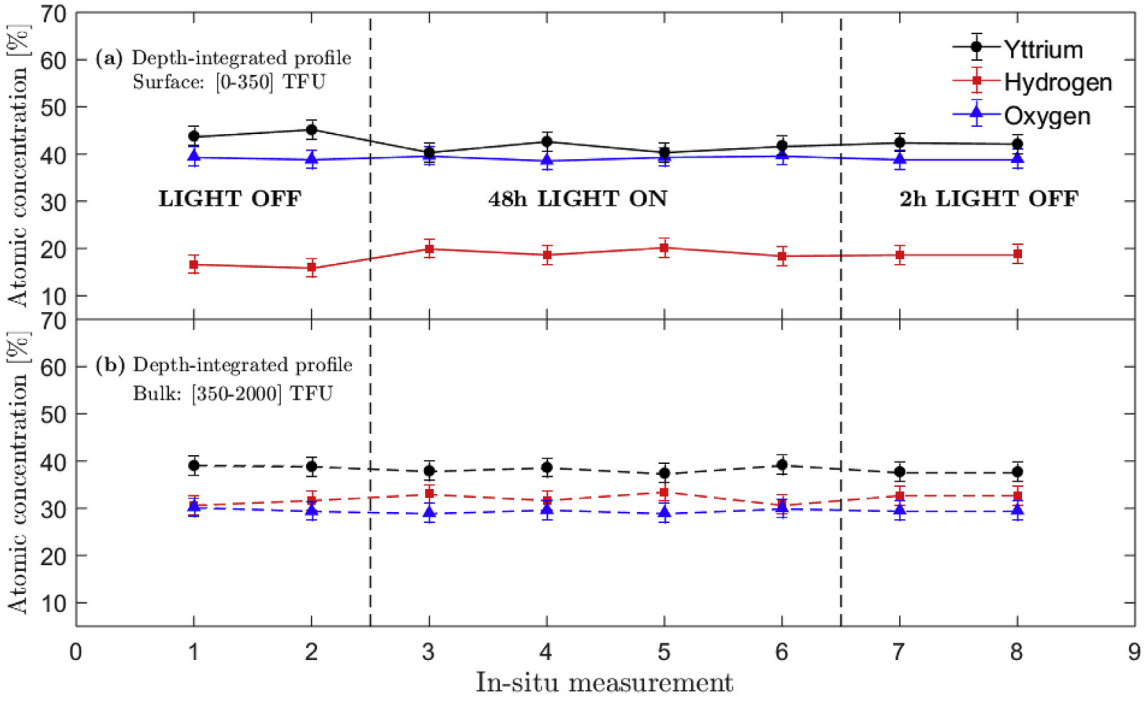

Fig. 3. (Color online). In-situ composition analysis of the YHO film during light illumination by ToF-E ERDA analysis. Eight spectra were recorded before, during and after light illumination in high-vacuum. The Y, H and O atomic concentrations in the corresponding depth-profiles deduced from the ToF-E ERDA were depth-integrated (a) close to the surface and (b) in the bulk of the sample. TFU = *Thin Film Units* = x 10^{15} at/cm^2. See text for details.

suggest that the photochromism observed for the investigated system is mainly related to either structural changes [11,13,14] and/or electronic rearrangements [15] than pronounced modifications of the overall composition of the material. Changes in the microstructure of the material with migration of species (such as O) from the bulk structure to grain boundaries and vice-versa during illumination and relaxation can in such a scenario explain all observations.

4. Summary and conclusions

The chemical composition of photochromic yttrium oxy-hydride thin-films, grown by reactive sputtering, was investigated by ion beam-based methods (RBS, PIXE, ToF-E ERDA and EBS). The quantitative analysis followed an interactive and self-consistent approach yielding to an unequivocal composition of the sample.

The investigated YHO films exhibit a thin oxygen-rich layer (≈30 nm) on the surface. Throughout the films, O is found to decreases from ≈55 at.% at the surface until ≈20 at.% at the interface film/substrate. Despite that, the yttrium concentration remains constant throughout the film; hydrogen shows an anti-correlated behavior with respect to oxygen with highest concentrations at larger depth, suggesting that O replaces H during the oxidation process. Light impurities (C and F) at cumulative concentrations of a few percent as well as heavy species (Fe and W) on the sub-percent level were detected.

In-situ investigations by ToF-E ERDA during light-illumination were performed and showed that photo-darkening can be triggered in a high-vacuum environment, while no significant change in composition (≥1.1 at.%) was observed. Time-resolved studies of the photochromic response in additional different ambients - performed also on samples of different thicknesses to further study the observed gradients - would be beneficial to further corroborate these interpretations. Furthermore, input from theory regarding the structural arrangements energetically

Table 1
Chemical composition of photochromic YHO thin film before, during and after illumination in high-vacuum deduced from in-situ ToF-E ERDA measurements. TFU = *Thin Film Units* = x 10^{15} at/cm^2.

Measurement	*In-situ Illumination*	*Time in HV [h]*	*Surface – [0–350] TFU [at. %]*			*Bulk – [350 – 2000] TFU [at.%]*		
			H	*O*	*Y*	*H*	*O*	*Y*
1	Off	1	16.7	39.5	43.8	30.7	30.3	39.0
2	Off	2	16.0	38.9	45.1	31.7	29.4	38.8
3	On	3.5	20.0	39.7	40.3	33.1	29.0	37.9
4	On	4.0	18.7	38.6	42.7	31.7	29.6	38.7
5	On	48.0	20.2	39.4	40.4	33.5	29.0	37.4
6	On	48.5	18.4	39.8	41.8	30.8	30.0	39.2
7	Off	53.0	18.7	38.8	42.5	32.7	29.5	37.7
8	Off	53.5	18.9	39.0	42.1	32.7	29.5	37.7
Average values [at.%]: ***BEFORE*** *illumination*			**16.3**	**39.2**	**44.5**	**31.2**	**29.9**	**38.9**
Standard deviation [at.%]			0.4	0.3	0.7	0.5	0.4	0.1
Average values [at.%]: ***UNDER*** *illumination*			**19.3**	**39.4**	**41.3**	**32.3**	**29.4**	**38.3**
Standard deviation [at.%]			0.4	0.3	0.6	0.6	0.2	0.4
Average values [at.%]: ***AFTER*** *illumination*			**18.8**	**38.9**	**42.3**	**32.7**	**29.5**	**37.7**
Standard deviation [at.%]			0.1	0.1	0.2	< 0.1	< 0.1	< 0.1

possible for different slightly alternating compositions would significantly advance the understanding of this kind of photochromic material.

Acknowledgments

The authors would like to acknowledge support by the Carl Tryggers foundation in form of a Postdoc scholarship (M.V.M.) as well as Swedish Institute Grant Visby Programme Scholarships for PhD studies (D.M.). Support by VR-RFI (contracts #821-2012-5144 & #2017-00646_9) and the Swedish Foundation for Strategic Research (SSF, contract RIF14-0053) supporting accelerator operation is gratefully acknowledged. The IFE group acknowledges financial support from the Research Council of Norway through the FRINATEK projects (240477/F20 to 287545) and from the internal project "Yttrium smart window" at Institution of Engineering and Technology (S-40073).

References

[1] J.N. Huiberts, R. Griessen, J.H. Rector, R.J. Wijingaarden, J.P. Dekker, D.G. de Groot, N.J. Koeman, Yttrium and lanthanum hydride films with switchable optical properties, Nature 380 (1996) 231–234.
[2] F.J.A. den Broeder, S.J. van der Molen, M. Kremers, J.N. Huiberts, D.G. Nagengast, A.T.M. van Gogh, W.H. Huisman, N.J. Koeman, B. Dam, J.H. Rector, S. Plota, M. Haaksma, R.M.N. Hanzen, R.M. Jungblut, P.A. Dunie, R.P. Griessen, Visualization of hydrogen migration in solids using switchable mirrors, Nature 394 (1998) 656–658.
[3] T. Mongstad, C. Platzer-Bjorkman, J.P. Maehlen, L.P.A. Mooij, Y. Pivak, B. Dam, E.S. Marstein, B.C. Hauback, S. Zh Karazhanov, A new thin film photochromic material: oxygen-containing yttrium hydride, Sol. Energy Mater. Sol Cells 95 (2011) 3596–3599.
[4] R.L. Sala, R.H. Gonçalves, R.H. Camargo, E.R. Leite, Thermosensitive poly(N-vinylcaprolactam) as a transmission light regulator in smart windows, Sol. Energy Mater. Sol. Cells 186 (2018) 266–272.
[5] T.H. Chang, H.C. Lu, M.H. Lee, S.Y. Kao, K.C. Ho, Multi-color electrochromic devices based on phenyl and heptyl viologens immobilized with UV-cured polymer electrolyte, Sol. Energy Mater. Sol. Cells 177 (2018) 75–81.
[6] K. Kanazawa, K. Nakamura, N. Kobayashi, Electroswitchable optical device enabling both luminescence and coloration control consisted of fluoran dye and 1,4-benzoquinone, Sol. Energy Mater. Sol. Cells 175 (2016) 42–53.
[7] F. Nafezarefi, H. Schreuders, B. Dam, S. Cornelius, Photochromism of rare-earth metal-oxy-hydrides, Appl. Phys. Lett. 111 (2017) 103903–103908.
[8] C.C. You, D. Moldarev, T. Mongstad, D. Primetzhofer, Max Wolff, E.S. Marstein, S. Zh. Karazhanov, Enhanced photochromic response in oxygen-containing yttrium hydride thin films transformed by an oxidation process, Sol. Energy Mater. Sol. Cells 166 (2017) 185–189.
[9] D. Moldarev, D. Primetzhofer, C.C. You, S. Zh, J. Montero Karazhanov, F. Martinsen, T. Mongstad, E.S. Marstein, M. Wolff, Composition of photochromic oxygen-containing yttrium hydride films, Sol. Energy Mater. Sol. Cells 177 (2018) 66–69.
[10] D. Moldarev, M.V. Moro, C.C. You, E.M. Baba, S. Zh Karazhanov, M. Wolff, D. Primetzhofer, Yttrium oxyhydrides for photochromic applications: correlating composition and optical response, Phys. Rev. Mater 2 (2018) 115203–115208.
[11] S. Cornelius, G. Colombi, F. Nafezarefi, H. Schreuders, R. Heller, F. Munnik, B. Dam, Oxyhydride Nature of rare-earth-based photochromic thin films, J. Phys. Chem. Lett. 10 (2019) 1342–1348.
[12] J. Montero, F.A. Martinsen, M. García-Tecedor, S. Zh, D. Maestre Karazhanov, B. Hauback, E.S. Marstein, Photochromic mechanism in oxygen-containing yttrium hydride thin films: an optical perspective, Phys. Rev. B 95 (2017) 201301–201304.
[13] C.V. Chandran, H. Schreuders, B. Dam, J.W.G. Janssen, J. Bart, A.P.M. Kentgens, P.J.M. van Bentum, Solid-state NMR studies of the photochromic effects of thin films of oxygen-containing yttrium hydride, J. Phys. Chem. 118 (2014) 22935–22942.
[14] J.P. Maehlen, T.T. Mongstad, C.C. You, S. Karazhanov, Lattice contraction in photochromic yttrium hydride, J. Alloy Compd 580 (2013) 119–121.
[15] M.P. Plokker, S.W.H. Eijt, F. Naziris, H. Schut, F. Nafezarefi, H. Schreuders, S. Cornelius, B. Dam, Electronic structure and vacancy formation in photochromic yttrium oxy-hydride thin films studied by positron annihilation, Sol. Energy Mater. Sol. Cells 117 (2018) 97–105.
[16] J.R. Tesmer, M. Nastasi, Handbook of Modern Ion Beam Materials Analysis, first ed., Materials Research Society, Warrendale, 1995.
[17] C.C. You, T. Mongstad, J.P. Maehlen, S. Zh, Karazhanov, Dynamic reactive sputtering of photochromic yttrium hydride thin film, Sol. Energy Mater. Sol. Cells 143 (2015) 623–626.
[18] W.K. Chu, J.M. Mayer, M.A. Nicolet, Backscattering Spectrometry, first ed., Academic Press INC, San Diego, 1978.
[19] C. Jeynes, J. Colaux, Thin film depth profiling by ion beam analysis, Analyst 141 (2016) 5944–5985.
[20] S.A.E. Johansson, J.L. Campbell, PIXE: A Novel Technique for Elemental Analysis, first ed., John Wiley & Sons, New York, 1988.
[21] J.R. Tesmer, C.J. Maggiore, M. Nastasi, J.C. Barbour, J.W. Mayer (Eds.), High Energy and Heavy Ion Beams in Material Analysis, Materials Research Society, Pittsburg, 1990.
[22] R.A. Jarjis, Nuclear Cross Section Data for Surface Analysis, Department of Physics, University of Manchester, 1979.
[23] P. Ström, P. Petersson, M. Rubel, G. Possnert, A combined segmented anode gas ionization chamber and time-of-flight detector for heavy ion elastic recoil detection analysis, Rev. Sci. Instrum. 87 (2016) 103303–103308.
[24] Y. Zhang, H.J. Whitlow, T. Winzell, I.F. Bubb, T. Sajavaara, K. Arstila, J. Keinonen, Detection efficiency of time-of-flight energy elastic recoil detection analysis systems, Nucl. Instrum. Methods B 149 (1999) 477–489.
[25] M. Rubel, H. Bergsåker, P. Wienhold, Ion-induced release of deuterium from co-deposits by high energy helium bombardment, J. Nucl. Mater. 241–243 (1997) 1026–1030.
[26] K. Monta, Y. Hasebe, A new model for release of hydrogen isotopes from graphite, J. Nucl. Mater. 176–177 (1990) 213–217.
[27] J. A. Leavitt, L. C. McIntyre Jr, M. D. Ashbaugh, J. G. Oder, Z. Lin and B. Dezfouly-Arjomandy, Cross sections for 170.5 backscattering of 4He from oxygen for 4He energies between 1.8 and 5.0 MeV, Nucl. Instrum. Methods B 44(199) 260–265.
[28] V. Paneta, M. Kokkoris, A. Lagoyannis, K. Preketes-Sigalas, Accurate accelerator energy calibration using selected resonances in proton elastic scattering and in (p,c) and (p,p0c) reactions, Nucl. Instrum. Methods B 406 (2017) 108–111.
[29] M. Mayer, W. Eckstein, H. Langhuth, F. Schiettekatte, U.V. Toussaint, Computer simulation of ion beam analysis: possibilities and limitations, Nucl. Instrum. Methods B 269 (2011) 3006–3013.
[30] J.L. Campbell, N.I. Boyd, N. Grassi, P. Bonnick, J.A. Maxwell, The Guelph PIXE software package IV, Nucl. Instrum. Methods B 268 (2010) 3356–3363.
[31] K. Arstila, J. Julin, M.I. Laitinen, J. Aalto, T. Konu, S. Kärkkäinen, S. Rahkonen, M. Raunio, J. Itkonen, J.-P. Santanen, T. Tuovinen, T. Sajavaara, Potku - new analysis software for heavy ion elastic recoil detection analysis, Nucl. Instrum. Methods B 331 (2014) 34–41.
[32] T.F. Silva, C.L. Rodrigues, M. Mayer, M.V. Moro, G.F. Trindade, F.R. Aguirre, N. Added, M.A. Rizzutto, M.H. Tabacniks, MultiSIMNRA: a computational tool for self-consistent ion beam analysis using SIMNRA, Nucl. Instrum. Methods B 371 (2016) 86–89.
[33] M.A. Arvizu, R.-T. Wen, D. Primetzhofer, J.E. Klemberg-Sapieha, L. Martinu, G.A. Niklasson, C.G. Granqvist, Galvanostatic ion detrapping rejuvenates oxide thin films, ACS Appl. Mater. Interfaces 7 (2015) 26387–26390.